

Remote sensing of the atmosphere of Mars using infrared pressure modulation and filter radiometry

D. J. McCleese, J. T. Schofield, R. W. Zurek, J. V. Martonchik, R. D. Haskins, D. A. Paige, R. A. West, D. J. Diner, J. R. Locke, M. P. Crisp, W. Willis, C. B. Leovy, and F. W. Taylor

The study of the atmosphere and climate of Mars will soon be advanced considerably by the Mars Observer mission. This paper describes the atmospheric sounder for this mission and how it will measure key Martian atmospheric parameters using IR gas correlation and filter radiometry. The instrument now under development will provide high-resolution vertical profiles of atmospheric temperature, pressure, water vapor, dust, and clouds using limb sounding techniques as well as nadir observations of surface thermal properties and polar radiative balance.

I. Introduction

The National Aeronautics and Space Administration has announced its intention to undertake a new mission to the planet Mars. Mars Observer is a low-cost mission focused on the study of Martian geoscience and climatology and utilizing a commercially available spacecraft.¹ A single spacecraft will be launched in 1990 and will enter a nearly circular 361-km altitude polar orbit around Mars in 1991. The Pressure Modulator Infrared Radiometer (PMIRR), described in this paper, has been selected for the Mars Observer mission and is under development at the Jet Propulsion Laboratory. PMIRR is a nine-channel limb and nadir scanning atmospheric sounder designed to address the climatology science goals of the mission. These are to determine the time and space distribution, abundance, sources, and sinks of Martian volatile materials and dust over a seasonal cycle and to explore the structure and aspects of the circulation of the Martian atmosphere. PMIRR employs filter and gas correlation radiometry primarily to map the 3-D time-dependent thermal structure of the atmosphere from the surface to 80 km, the atmospheric dust load-

ing and its global, vertical, and temporal variation; the seasonal and spatial variation of the vertical distribution of atmospheric water vapor and to distinguish between CO₂ and H₂O condensates in the atmosphere and map their spatial and temporal variation.

II. Measurement Approach

This section describes the measurement approach adopted to meet these objectives. The reasons for the selection of particular experimental techniques and the constraints that these techniques place on the hardware design are also discussed.

A. Limb Sounding

Because of many shared objectives, properties, and phenomena, the study of the earth's upper atmosphere serves as a paradigm for investigation of the atmosphere of Mars. Over the past two decades, research into the nature of the terrestrial stratosphere and mesosphere has progressed from an initial phase of exploration to the focused studies now in progress which utilize specialized remote sensing instruments on orbiting platforms. Detailed studies of the upper atmosphere are undertaken largely by limb viewing experiments. The most recent and successful of these are the Limb Infrared Monitor of the Stratosphere (LIMS)² and the Stratospheric and Mesospheric Sounder (SAMS),³ both on the Nimbus 7 satellite. Together these instruments employed filter and pressure modulation radiometry to map the global distribution of temperature, O₃, HNO₃, H₂O, CH₄, CO, N₂O, NO, and NO₂ in the earth's upper atmosphere with high vertical resolution.

The vertical resolution of a passive remote sounding measurement is determined by the pressure dependence of atmospheric opacity in the wavelength inter-

F. W. Taylor is with University of Oxford, Department of Atmospheric Physics, Clarendon Laboratory, Oxford, U.K.; C. B. Leovy is with University of Washington, Department of Atmospheric Sciences, Seattle, Washington 98195; the other authors are with Jet Propulsion Laboratory, 4800 Oak Grove Drive, Pasadena, California 91109.

Received 16 January 1986.

0003-6935/86/234232-14\$02.00/0.

© 1986 Optical Society of America.

val selected. In theory, limb viewing geometry gives a factor of 6.5 advantage in vertical resolution over nadir viewing. At best, the resolution of a nadir measurement can approach the atmospheric scale height, whereas that of a limb measurement is limited in practice by its field of view. Limb sounders achieve better than one-half of the scale height vertical resolution in current flight systems. Limb sounding significantly enhances species sensitivity by increasing the geometrical optical path of the measurement, by a factor of 45 in the case of Mars. Also, the species sensitivity of a limb sounder is not dependent on the vertical atmospheric temperature gradient. For example, as the surface and atmosphere become more nearly isothermal, errors in profiles and abundances derived from nadir emission measurements increase rapidly although limb measurements are unaffected. Such conditions are far from rare in either the terrestrial or Martian atmospheres.

The similarities between the Martian atmosphere and the terrestrial upper atmosphere, and the success of the remote sensing techniques discussed above, have led to the choice of limb sounding as the primary operating mode of PMIRR, although it also has a nadir scanning capability for surface observations. The vertical resolution of PMIRR for all limb mode measurements, determined by its field of view, is set to 5 km or half of the Martian atmospheric scale height. The line of sight horizontal resolution in the limb sounding mode is 240 km compared with the orbit separation of ~1650 km at low latitudes. This provides a longitudinal (28°) and latitudinal (4°) resolution, which is well suited to observations of synoptic-scale climatological fields.

B. Pressure Modulation Radiometry

Gas correlation spectroscopy is particularly appropriate for measurements of the atmosphere of Mars because it is species specific. Radiation originating from the ever present ubiquitous airborne dust can be distinguished from that originating from the gas of interest.

Pressure modulation radiometry is a novel application of gas correlation spectroscopy.⁴ The technique detects radiation from the emission lines of a specific radiatively active atmospheric constituent gas by modulating the pressure of the same gas in a cell placed in the optical path of the instrument. The transmission of the pressure modulator cell (PMC), and hence the intensity of atmospheric radiation incident on the detector, varies at the frequency of modulation only near gaseous absorption lines. The signal at the modulation frequency, selected by electronic processing, therefore, quantifies atmospheric emission in spectral regions in and near the gaseous absorption lines in the PMC, which match line for line the emission lines of the same gas in the atmosphere.

The spectral response of a pressure modulator radiometer (PMR) can be designed to fit the shape of atmospheric line profiles by varying cell length, mean

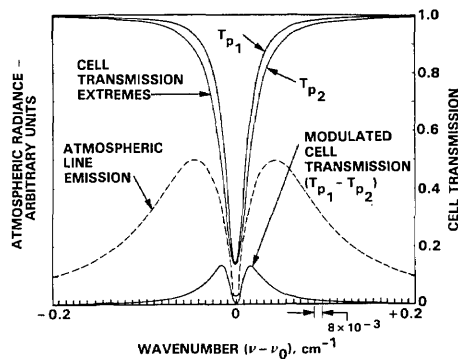


Fig. 1. Spectral discrimination of a PMR for the water vapor line at $1375.0879 \text{ cm}^{-1}$. Atmospheric emission is calculated for a limb view of the Martian atmosphere at 4-km tangent height using the Cospar standard model temperature profile and a 35-pr. μm column abundance of uniformly mixed water vapor. The pressure modulator cell is 10 cm long and contains H_2O at a mean temperature of 300 K modulated between pressures of $P_1 = 16.0$ and $P_2 = 21.4$ mbar.

pressure, and modulation depth. Once chosen, cell length is fixed, but pressure and modulation depth can be altered in flight. Mean cell pressure is regulated by a thermally controlled molecular sieve gas reservoir attached to the pressure modulator. The spectral resolution of a PMR is limited only by the Doppler width of lines in the PMC, which is typically 10^{-3} cm^{-1} at 1000 cm^{-1} . Because a PMR channel is defined by a broad bandpass filter, 50–100 lines can be observed simultaneously giving the PMR a multiplex advantage. Furthermore, instrument etendue is not limited by the high-resolution element, and the PMR is, therefore, able to collect a great deal more energy than an interferometer of comparable resolution.⁵

Figure 1 illustrates the spectral discrimination achieved by pressure modulation radiometry for a single line in the Martian atmosphere within the bandpass of a spectral filter. The curves labeled T_{p_1} and T_{p_2} show the transmission of the PMC at the two extremes of the modulator pressure cycle. The curve labeled $T_{p_1} - T_{p_2}$ is the effective transmission of the PMC sampled at the modulation frequency within the narrow spectral interval shown.

In any PMR channel, in addition to the modulated signal, there is an unmodulated signal component for which the detector views the atmosphere through the PMC at its effective mean pressure. This unmodulated or wideband signal provides a measure of uncorrelated scene radiation while largely rejecting atmospheric emission corresponding to the gas contained in the cell. In PMIRR, incident radiation is mechanically chopped at 800 Hz to allow electronic processing of the wideband signal. The pressure modulated signal appears as a 50-Hz amplitude modulation on the 800-Hz wideband signal.

Figure 2 illustrates the ability of pressure modulation radiometry to detect gaseous emission selectively in the presence of foreign line and continuum emission. It shows the emission spectrum of Mars that would be seen by an infinite-resolution limb viewing spectrometer for a tangent height near the surface over a narrow

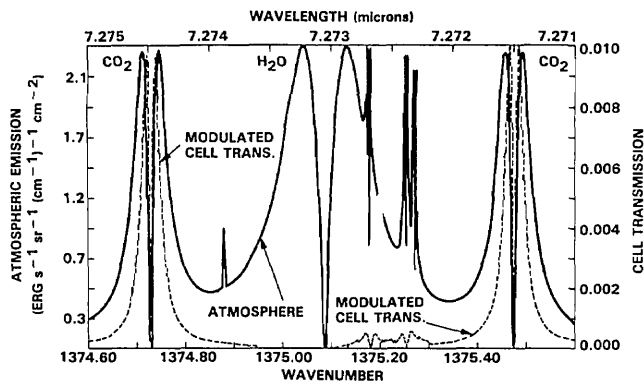


Fig. 2. Spectral selectivity of a PMR for a Mars limb view at 5-km tangent height. The standard model temperature profile is used together with a uniform H₂O mixing ratio of 10⁻³ (71 pr. μm). The cell is 4 cm long and contains CO₂ at 300 K modulated between 65 and 125 mbar. The CO₂ isotope mixture ratio ¹²C¹⁶O₂:¹²C¹⁶O¹⁸O:¹²C¹⁸O₂ is 4:4:1.

spectral interval within the bandpass of a PMIRR temperature sounding channel using a PMC containing CO₂. Although both CO₂ and H₂O lines are present, it can be seen from the figure that the PMC selectively detects CO₂ lines while largely ignoring H₂O and continuum features. The inverted centers of the CO₂ and H₂O emission lines are a consequence of their large optical depth in the limb path and the positive lapse rate of the atmosphere between the limb tangent height and level of line formation.

C. Temperature Sounding

Daily mapping of the global 3-D temperature field from the Mars Observer is the primary measurement objective of the PMIRR experiment. Temperature measurements characterize directly the stability, saturation state, and structure of the Martian atmosphere and can be used to derive atmospheric circulation, transport, and energy and momentum budgets.⁶

Emission from the spectral features of carbon dioxide has traditionally been exploited for remote temperature sounding by IR filter and pressure modulation radiometry in the terrestrial atmosphere.⁷ Carbon dioxide was chosen for its stability, known constant mixing ratio, well-understood spectroscopy, and the location of its emission features near the peak of the Planck function for typical atmospheric temperatures. For the same reasons, CO₂ is ideal for temperature sounding in the atmosphere of Mars, particularly as it is the dominant constituent with a volume mixing ratio of 0.95. PMIRR has three temperature sounding channels which share a single PMC, 4 cm in length, containing 80 mbar of CO₂.

To sound temperature effectively in the lower atmosphere, where CO₂ amounts in the limb path are extremely large, measurements are made near 7 μm in the weak fundamental ν₁ band of ¹²C¹⁶O¹⁸O. The weak band and the relative isotopic abundance of 0.004 give, for a limb path with a tangent height at the surface, an effective optical depth of unity for the pressure modu-

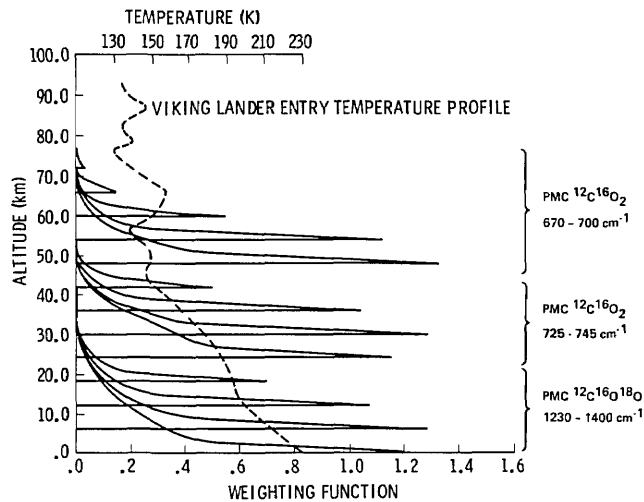


Fig. 3. Vertical response of PMIRR for limb temperature sounding. The cell conditions are those of Fig. 2. The vertical response or weighting function is defined here by $K(z) = [\partial T(z, \infty) / \partial z] \times 10$, where $T(z, \infty)$ is the effective transmission from level z to space.

lated signal component. By enhancing the relative abundance of ¹²C¹⁶O¹⁸O in the PMC, this signal can be proportionally increased. The isotopic ratios used are ~4/9 ¹²C¹⁶O₂, 4/9 ¹²C¹⁶O¹⁸O, 1/9 ¹²C¹⁸O₂, increasing the pressure modulated signal component by a factor of 110. Models derived from Mariner 9 data indicate that 7 μm is also a region of minimum dust extinction in the Martian atmosphere.⁸ Temperature sounding in the middle atmosphere (20–50 km), where CO₂ amounts in the limb path are smaller, is achieved by a channel in the wing of the 15-μm ν₂ band of CO₂, and above 50 km a channel at the band center is used. Extinction by airborne dust at these altitudes is generally small.

Vertical temperature profiles are derived from measurements made by PMIRR during stepped scans of the Martian limb. Each limb scan consists of 5-km vertical steps providing contiguous coverage of the atmosphere from 0 to 80 km. Figure 3 shows the vertical response or weighting functions corresponding to a single limb scan for the three PMIRR temperature sounding channels together with their spectral assignments.

D. Airborne Dust and Condensate Measurements

Airborne dust is second only to temperature in importance for the detailed study of the atmosphere of Mars. It is the primary absorber of solar radiation in the atmosphere and thus provides a major thermodynamic drive for the Martian circulation. Figure 4 illustrates the variability of vertical column dust opacity at visible wavelengths over one Martian year derived from measurements at the two Viking lander sites.⁸ Observations made by instruments on the Mariner 9 and Viking spacecraft have shown that the IR opacity of airborne dust is strongly spectrally dependent^{9,10} and have allowed opacities at IR and visible wavelengths to be related.¹¹ For example, optical

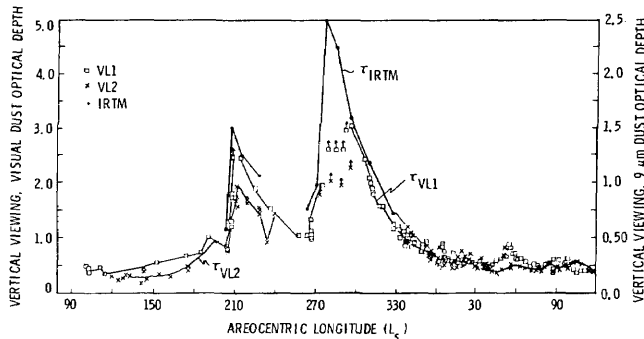


Fig. 4. Variation of vertical dust opacity in the Martian atmosphere over one Mars year derived from measurements at the Viking Lander 1 and 2 sites. The period includes a global dust storm.

depth at $7 \mu\text{m}$ is a factor of 10 less than at visible wavelengths. Models derived from these observations have been used to guide the selections of PMIRR channels, although the analysis of PMIRR data is not dependent on *a priori* assumptions of dust spectral characteristics.

PMIRR measures aerosol opacity as a function of altitude in eight spectral intervals between 6.5 and $50 \mu\text{m}$. This information is obtained from limb emission observations made simultaneously and with the same vertical and horizontal resolution as the temperature measurements. Spectral channels at 11.8 and $20.6 \mu\text{m}$ are chosen for their sensitivity to small amounts of dust and H_2O ice, which is known to be present in the atmosphere. A channel at $31.7 \mu\text{m}$ serves as a reference for total line-of-sight opacity due to airborne particulates as it is located in a spectral interval where opacity is influenced little by gaseous absorption. Finally, a $46.5\text{-}\mu\text{m}$ channel is relatively insensitive to dust and condensate particles having the sizes and number densities expected in the Martian atmosphere.

Given the vertical profile of temperature as a function of pressure, profiles of dust and condensate extinction coefficients can be derived from limb and nadir emission measurements made in each PMIRR infrared channel during a limb scan. Two processes contribute to the emitted radiance: thermal emission by gas and particulates and scattering by particulates. The primary scattering of upwelling radiation from the surface dominates the scattering source function as the particle single-scattering albedo is small, and multiple scattering is negligible at these wavelengths. The effects of primary scattering and emission and extinction by gas and particulates are accounted for by a modified emissivity growth approximation technique¹² used successfully to retrieve profiles of sulfuric acid aerosol mass loading in the terrestrial stratosphere from Solar Mesosphere Explorer limb radiance measurements.¹³ The resulting multispectral extinction data can then be used to distinguish between dust and condensate aerosols and to examine their microphysical properties.

The independent retrieval of temperature in the presence of dust is essential to this approach and is made possible by the two signal components of the CO_2

pressure modulator temperature sounding channels. The contrast in CO_2 optical depth in the atmospheric path for the wideband and pressure modulated signal components allows thermal emission from aerosols and CO_2 to be differentiated. Because both components have the same spectral bandpass and have coincident weighting functions when the atmosphere is not optically thick, the ratio of the measured radiances associated with each component is almost equal to the ratio of atmospheric emissivities and is insensitive to temperature. The emissivities of a limb path for the two signal components can be calculated given the known spectroscopy of CO_2 . For a particular channel and pressure level, the emissivity ratio $\epsilon_{\text{pressure modulated}}/\epsilon_{\text{wideband}}$, and hence the radiance ratio, has a unique value. However, the presence of aerosols in the limb path alters the ratios expected for CO_2 alone. The radiance ratio is, therefore, a sensitive measure of line-of-sight aerosol opacity, so that the contribution of aerosols to the observed radiances can be incorporated into the temperature retrieval scheme.

E. Water Vapor Measurements

Water appears to have played a crucial role in modifying the surface of Mars in the past,¹⁴ and knowledge of its present seasonal cycle may provide the key to understanding past Martian climates. Water vapor profiles measured with good horizontal, vertical, and temporal resolution reveal the nature of transport processes and the distribution of sources and sinks of water.

PMIRR employs a pressure modulator cell 10 cm in length containing 18 mbar of H_2O to sound water vapor in the atmosphere of Mars. Measurements are made at $6.9 \mu\text{m}$ in the near wing of the water vapor ν_1 vibration-rotation band and are simultaneous and collocated with temperature measurements. As is the case for temperature measurements, the signal in this channel contains pressure modulated and wideband components which permit the extraction of both water vapor and dust optical depths, given the temperature profile.

F. Pressure Measurements

Pressure is an important climatological variable for Mars where a sizable fraction of the total atmospheric mass condenses annually at the winter pole. Furthermore, for many diagnostic studies, the measurement of climatological variables such as temperature is most conveniently referenced to constant pressure levels. Pressure is also the only absolute vertical scale to which remote sounding measurements can be referenced when spacecraft attitude is uncertain.

The tangent pressure for a given limb view can be derived from the pressure modulated and wideband signal components of the temperature sounding CO_2 pressure modulator channels of PMIRR, provided path opacity is dominated by CO_2 . Measurements at $14.6 \mu\text{m}$ in the $30\text{--}50\text{-km}$ region give the best results because of high SNRs and generally negligible dust opacity. The ratio of the two signal components is a

strong function of tangent pressure but is insensitive to atmospheric temperature. Pressure and temperature can, therefore, be retrieved simultaneously with an accuracy that is limited by SNRs and the precision with which conditions in the PMC and CO₂ spectroscopy are known. The pressure retrieval capabilities of PMIRR are very similar to those of earth orbiting limb sounders. For example, the SAMS instrument on Nimbus 7 retrieved pressures to ~1.5% using temperature sounding CO₂ pressure modulator channels.³ PMIRR can achieve similar accuracies at Mars.

Given pressure in the 30–50-km range, pressure at other levels can be derived from the hydrostatic equation using the retrieved temperature profile and the accurate relative altitude scale associated with the PMIRR limb scan steps. Retrieved temperature, aerosol, and water vapor profiles can then be referenced to simultaneous and collocated pressure scales. Surface pressure can be derived from PMIRR measurements of the Martian limb if attitude knowledge and Martian geoid data are available.

G. Surface Measurements

In addition to its atmospheric observations PMIRR also obtains data on polar radiative balance, CO₂ frost deposits, and surface thermal inertia, building on the results from the Viking IRTM experiment.¹⁵ The annual polar heat balance is one of the most important aspects of the Martian climate system. It can control the partitioning of available CO₂ between atmosphere, polar caps, and regolith and is strongly influenced by astronomical variations in the distribution of incident solar radiation through feedback effects involving the seasonal cycles of water vapor and dust. CO₂ frost deposits on Mars are important because their spatial and temporal distribution is a sensitive indicator of interannual climate variations, and thermal inertia measurements provide a means of determining the distribution of sand, dust, and exposed rock on the surface.

PMIRR provides accurate dayside and nightside surface brightness temperatures in the 6.8–50- μm wavelength range at high spatial resolution and with simultaneous measurements of broadband solar reflectance and the properties of the overlying atmosphere. The 0.3–3.0- μm spectral response of the PMIRR solar channel encompasses over 97% of the incident solar flux, and its observations are used to construct hemispheric bidirectional reflection plots and determine albedos on a daily basis for the core regions of the north and south permanent caps.¹⁶ The IR channel observations are used to synthesize daily polar emission spectra as a function of zenith angle and hence derive net emission by angular integration.¹⁶ Errors introduced by the necessary interpolation and extrapolation of emission spectra are small because the spectral features that make the greatest contribution to the bolometric integral are well sampled by PMIRR.¹⁷ Figure 5 shows the location of the PMIRR infrared channels in relation to the cumulative Planck functions for 150 and 300 K blackbodies. Errors are

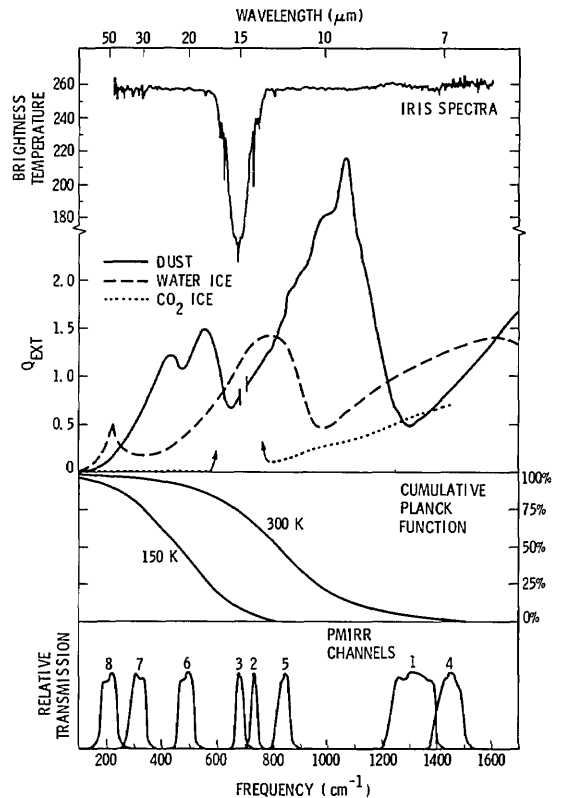


Fig. 5. PMIRR spectral channel locations compared with cumulative Planck functions, the spectral characteristics of Mars atmospheric components, and a typical Mariner 9 IRIS spectrum.

further reduced by using the overlying atmospheric properties, determined simultaneously by PMIRR, in emission spectrum synthesis. Albedo and net emission characterize polar heat balance, which is determined primarily by the net flux of solar and IR radiation at the top of the atmosphere.^{17,18}

CO₂ frost deposits can be identified by their temperature which is always close to the CO₂ solid-vapor equilibrium temperature (~148 K at 6-mbar partial pressure). PMIRR detects surface frost by measuring surface brightness temperatures at 31.7 and 46.5 μm . These channels are insensitive to the presence of dust and water ice particles in the overlying atmosphere and do not exhibit a nonlinear response to the presence of hot, unfrosted material in the field of view. Surface temperatures from these channels can also be used in conjunction with calibrated solar reflectance observations to determine global thermal inertias on a scale of $2 \times 2^\circ$ in latitude and longitude every 56 days.

III. Observational Strategy

The Mars Observer provides a three-axis stabilized platform in a 361-km sun-synchronized polar orbit about Mars. The spacecraft crosses the equator at 2 p.m. and 2 a.m. local time and completes ~12.7 orbits/day. Subspacecraft tracks on successive orbits are separated by 28.4° longitude.

For each Mars Observer orbit, PMIRR measures both day and nighttime meridional cross sections of

atmospheric properties from 0 to 80 km and the variation of surface properties along the subspacecraft track. It achieves its observational goals by employing a two-axis elevation-azimuth scan mirror to obtain nadir off-nadir, limb, and space views in the fields of view of all its channels.

The instantaneous field of view of each PMIRR detector is 3.1×15.6 mrad. From the Mars Observer orbit this gives a 5-km vertical by 25-km horizontal footprint at the limb of Mars and a 1-km in-track by 5-km cross-track footprint in the nadir. For limb sounding there is also a horizontal line-of-sight dimension to the field of view of ~ 240 km centered approximately at the tangent point and determined by the atmospheric scale height and curvature of Mars.

A number of automatic scan mirror cycles are available to PMIRR, covering nominal mapping, calibration, and specialized observation modes. The principal mode is the nominal mapping mode, illustrated in Fig. 6, which is composed of alternate in-track limb scans and nadir views interspersed in a repetitive cycle. The limb scan consists of soundings at twelve 5-km steps, each with a 2-s dwell time, to obtain continuous coverage for each detector field of view over a 60-km height range. The spacecraft pointing stability does not significantly degrade the instrument 5-km vertical field of view. All the detector fields of view occupy one of three positions which are scanned together across the limb. The channel positions at the start of a scan are shown in Fig. 6. This arrangement gives a total vertical coverage ranging from -20 to 80 km and allows individual channels to span the necessary height range while accommodating uncertainties in spacecraft attitude control. Channels 6 and 7 each have two detectors and hence two fields of view. Following the limb scan, the scan mirror slews to the nadir position to obtain a single sounding of the atmosphere and surface. The mirror then slews back to the limb, and the entire cycle repeats. The full sequence occupies 28 s and, given the 3.38-km/s spacecraft velocity, results in a 95-km horizontal displacement between successive limb profiles and adjacent nadir soundings.

IV. Instrumentation

The bandpass, type, and function of the PMIRR spectral channels required to meet the objectives discussed above are summarized in Table I. Figure 7 shows the mechanical configuration of PMIRR with major components indicated. Its chief physical and operational parameters are listed in Table II. An artist's rendering of the flight instrument is shown in Fig. 8.

A. Optics

The nine PMIRR channels summarized in Table I are delineated by the optical layout shown schematically in Fig. 9. All channels share a common scan mirror and telescope primary and view Mars and space alternately at 800 Hz via a rotating double-sided mirror chopper. The CO_2 and H_2O PMCs are located in the optical path of channels 1-4 and impart a low-

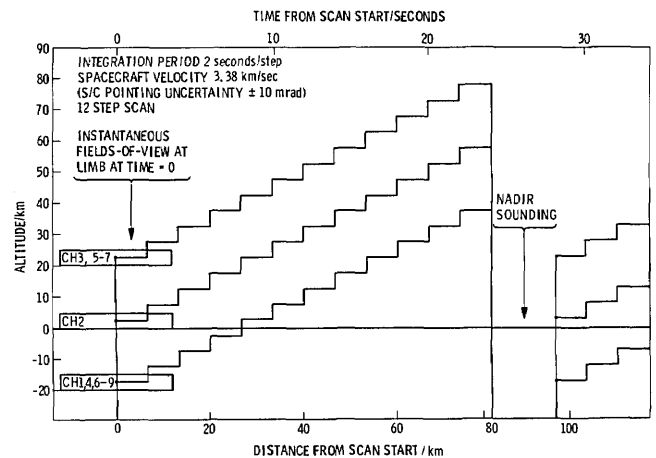


Fig. 6. Instantaneous PMIRR fields of view at the limb of Mars together with the limb/nadir scan pattern for the nominal mapping observation mode.

frequency (50-Hz) amplitude modulation to the 800-Hz chopped signal. Individual channels are defined by spatial beam splitters, dichroics, spectral bandpass filters, and the spectral response of their detectors. All optical components, including the PMCs, are maintained at the instrument ambient temperature of 300 K with the exception of the channel 1-5 bandpass filters at 140 K, condensing optics at 80 K, and HgCdTe detectors at 80 K, which share a common focal plane assembly cooled by a passive radiative cooler.

The goal of the optical design is to provide accurately located high spatial definition fields of view in nine spectral intervals. PMIRR uses a 6-cm aperture $f/11.9$ Gregorian telescope. Radiation from Mars is directed alternately between two secondary mirrors by the reflective chopper positioned at the primary focus of the telescope. The aperture stop for each instrument channel is positioned at the condensing optics, and the field stop is defined by the active area of its $150 \times 750\text{-}\mu\text{m}$ detector. It is particularly important to have good image quality in the $150\text{-}\mu\text{m}$ dimension, which corresponds to altitude at the limb of Mars. The aperture and field stops of channels 1-4 are reimaged at the entrances and exits of the PMCs. This arrangement allows channel etendue to be maximized for a given PMC length and volume.

Channels 1-3 view Mars through the CO_2 PMC and are separated by an image dissector mirror at the field plane behind the cell. Channels 4-9 are separated by germanium and silicon dichroics. Plane folding mirrors are used to position channels 1-5 on the $5 \times 6\text{-cm}$ cold focal plane with the correct image rotation. All mirrors seen by the broadband albedo channel 9 are aluminum coated, whereas the remainder are gold coated. Doublet condenser lenses are utilized by all the channels except 6 and 9, which employ Schwarzschild objectives to minimize material absorption and ensure a flat spectral response. Channels 1-5 use germanium doublets, and the remainder are of silicon. Substrates for windows and bandpass filters are made

Table I. PMIRR Channel Spectral Characteristics and Measurement Functions

CHANNEL NUMBER	BANDPASS - cm^{-1}	CENTRAL WAVELENGTH μm	CHANNEL TYPE (1)	MEASUREMENT FUNCTION
1	1,230 - 1,400	7.6	PMR(CO_2) + WB	TEMPERATURE 0-20 km
2	725 - 745	13.6	PMR(CO_2) + WB	TEMPERATURE 20-50 km
3	670 - 700	14.6	PMR(CO_2) + WB	PRESSURE 30-50 km & TEMPERATURE 50-80 km
4	1,400 - 1,500	6.9	PMR(H_2O) + WB	WATER VAPOR 0-35 km
5	820 - 870	11.8	WB	DUST AND CONDENSATES 0-80 km. RADIATIVE BALANCE
6	460 - 510	20.6	WB	
7	290 - 340	31.7	WB	
8	190 - 240	46.5	WB	
9	3,333 - 33,333	0.55	WB	

(1) PMR DENOTES A RADIOMETER CHANNEL WHICH USES A PRESSURE MODULATOR CELL CONTAINING THE SPECIFIED GAS. WB DENOTES A WIDEBAND OR FILTER CHANNEL.

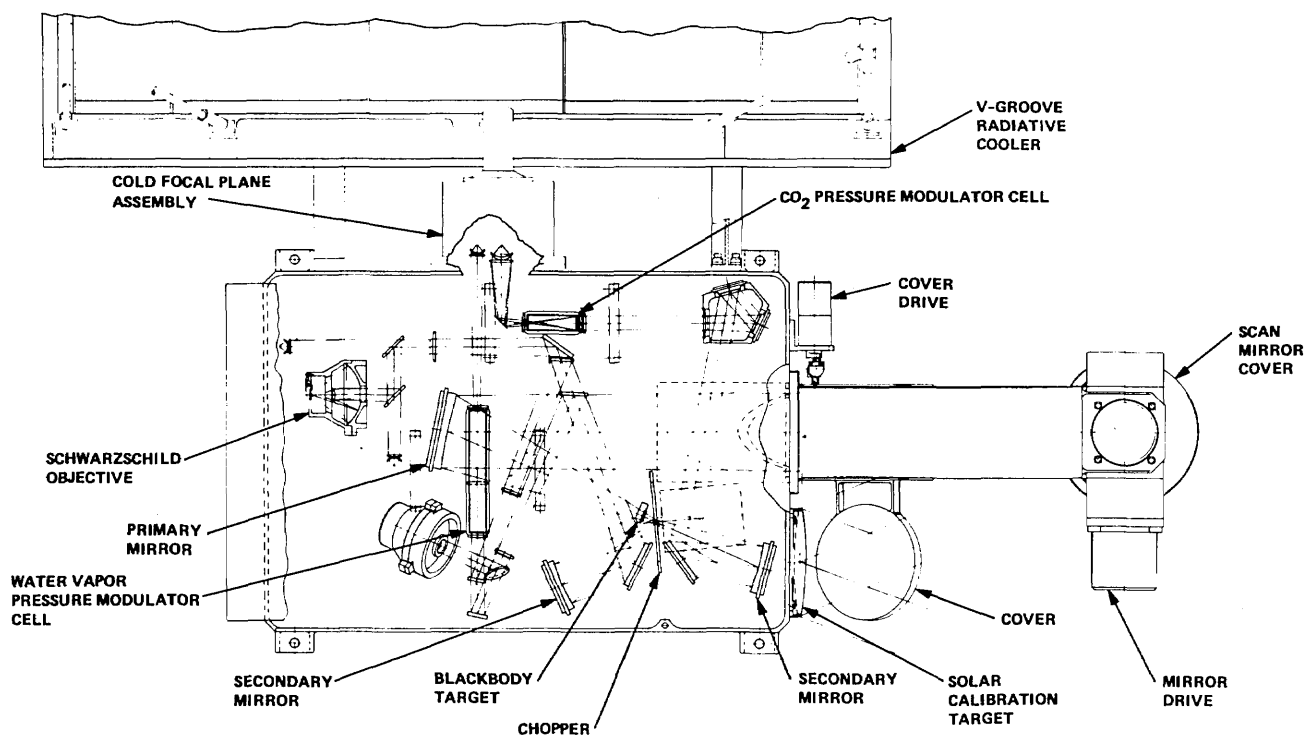


Fig. 7. Mechanical configuration of the PMIRR instrument and optical bench.

of germanium or zinc selenide for channels 1-5, silicon for channels 6-8, and calcium fluoride for channel 9. Optical alignment is facilitated by the largely coplanar optical design, precision machining, and the use of ZnSe components where possible.

The most important optical mechanisms in PMIRR are the scan mirror and chopper assemblies. The scan mirror assembly enables PMIRR to operate in the diverse observation modes discussed above. Elevation and azimuth drive actuators are mounted orthog-

Table II. PIMRR Instrument Summary

Instrument parameter	Value
Telescope aperture	6-cm diameter 28.3-cm ² area
Field of view	0.18 × 0.90° (detector) 1.6 × 0.90° (instrument)
Etendue (AΩ)	1.5 × 10 ⁻³ cm ² · sr (detector) 1.35 × 10 ⁻² cm ² · sr (instrument)
Integration period	2 s
Data rate	120 bits/s science 30 bits/s housekeeping
Mass	25.7 kg
Power	27.1 W
Dimensions	81 × 33.5 × 24 cm instrument 70 × 40 × 63 cm cooler

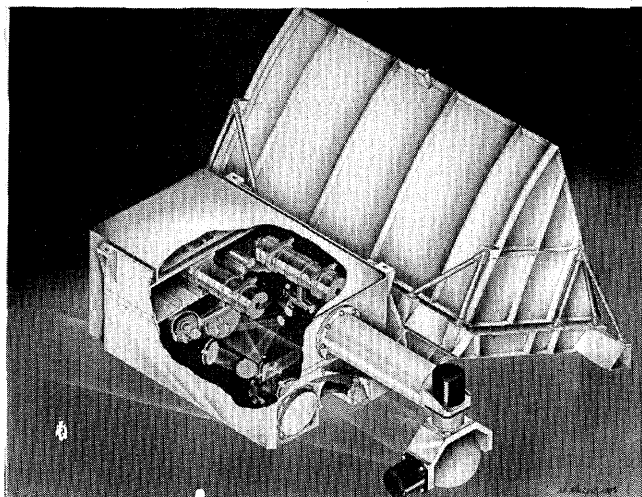


Fig. 8. Artist's rendering of the Pressure Modulator Infrared Radiometer. Part of the instrument housing is cut away to reveal major instrument components.

onally in a yoke arrangement (Fig. 7). The actuators are 4.5° permanent magnet stepper motors coaxially linked to 100:1 harmonic drive speed reducers. The system provides elevation and azimuth steps of 0.045°, displacing a detector field of view by 0.09° or half its width and slew rates of 31.25°/s in both elevation and azimuth.

The chopper assembly provides 100% signal modulation at 800 Hz over the life of the mission. This is achieved by an 8.4-cm diameter, twelve-toothed, double-sided mirror disk rotating at 67 Hz (Fig. 7). The mirror is 2 mm thick, machined from the low-thermal expansion material Zerodur, and driven by an ac hysteresis, synchronous, two-phase, 28-V, 400-Hz motor.

B. Provisions for Radiometric Calibration

Provisions for accurate radiometric calibration play a major role in the PMIRR optical design. The objective is an absolute radiometric accuracy of 0.5% in the thermal IR channels and 3% in the broadband albedo channel. High radiometric precision is achieved for all the channels by chopping target radiation viewed via the scan mirror to cold space at 800 Hz. Radiometric accuracy is obtained from two calibration targets,

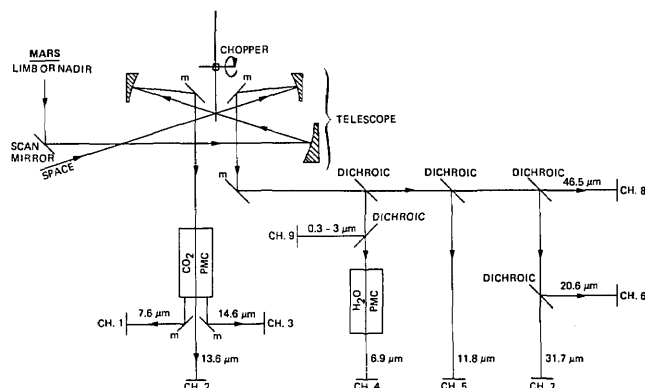


Fig. 9. PMIRR schematic optical layout.

again chopped against cold space. The first is cold space itself, viewed via the scan mirror, and the second is a 300 K blackbody that can be introduced by an actuator into the optical path of the instrument just in front of the prime focus of the telescope. The scan mirror, primary mirror, chopper, and optical bench temperatures are also controlled at 300 K to minimize calibration drifts. During a calibration cycle, the scan mirror moves to permit all the channels to view cold space, then the blackbody, following which the instrument returns to its current observation mode.

An additional calibration source is required for the broadband albedo channel. This is supplied by a diffusely scattering target mounted on the front of the instrument enclosure. The target is viewed via the scan mirror when the orbiter crosses the polar terminator of Mars. It fills the instrument field of view and aperture and is protected against contamination by a removable cover throughout the launch, cruise, and orbital insertion phases of the mission.

C. Detectors and Cooled Focal Plane Assembly

The nine PMIRR channels employ single-element detectors. Channels 1-5 in the 7-15-μm spectral interval use HgCdTe photon detectors cooled to 80 K on a common focal plane assembly, whereas the solar and 20-50-μm channels 6-9 employ deuterated triglycine sulfate (DTGS) detectors at the PMIRR ambient temperature of 300 K and have separate focal planes. Channels 1 and 4 have photovoltaic HgCdTe detectors, and the remaining cooled detectors are photoconductive. All channels are detector noise limited with the exception of channels 1 and 4 which are instrument background limited.

Channels 1-5 cold focal plane assembly (CFPA) consists of detectors, condensing optics, their mounting structures, and a thermal control heater and sensor. The CFPA is maintained at 80 K by the cold stage of a passive radiative cooler. It is suspended within a detector housing, cooled to 140 K by the cooler intermediate stage. A critical factor that has driven the cold optics design is the need to minimize background radi-

severe disadvantage with respect to flight proven operating life and power consumption.²⁰

The PMIRR instrument design incorporates a two-stage passive radiative cooler. The component heat loads from the CFPA, and its enclosure which the cooler must radiate is ~ 90 mW at the cold stage (80 K) and 750 mW at the intermediate stage (140 K). In addition the radiator must also dissipate parasitic heat loads from the warmer parts of the instrument and cooler as well as externally absorbed diffusely scattered solar and planetary radiative fluxes. The nature of the mission profile requires that the radiative cooler have a reclosable door to prevent contamination of cold surfaces. When open, this door also acts as a planet shield.

E. Pressure Modulators

The PMIRR pressure modulators provide a robust low-power flight proven means of mechanically modulating the amount of gas in an optical cell, using dynamically balanced pistons driven electromagnetically at resonance within a sealed unit.⁴ The pistons are suspended from diaphragm springs within the modulator, and, because they are driven at resonance, their frequency of oscillation is an accurate measure of mean cell pressure. At the pressures selected for the PMIRR modulators, piston resonant frequency is ~ 50 Hz. Mean cell pressure is controlled by a thermostatically regulated molecular sieve gas reservoir, which holds several hundred times the amount of gas present in the modulator and is an effective buffer against long-term adsorption.

F. Electronics and Signal Processing

Figure 10 is a block diagram illustrating the key electronic elements of PMIRR. These elements perform functions that can be classified into the categories of power conversion and regulation, digital logic control and data processing, mechanism control, temperature regulation, housekeeping data monitoring, and signal processing.

The digital logic control and data processing electronics interface with the spacecraft payload data subsystem (PDS), receiving and executing commands and processing science and engineering data. A microcomputer is used for executive control, for example, to implement an automatic PMIRR scan mirror cycle. The primary program resides in ROM and is copied into RAM at turn-on. Modification and backup of the main program are accomplished by linking it to changes made in RAM through small-scale memory loads.

A series of radiometers developed by Oxford University for measurements from stratospheric balloons²¹ used the same signal processing techniques as those planned for PMIRR. The PMR channels process a doubly chopped signal that is 100% modulated by the

chopper at 800 Hz and is then amplitude modulated by a PMC at ~ 50 Hz. This is achieved by wideband and sideband amplifiers. The wideband amplifier processes the 800-Hz filter radiometer signal and consists of a gain adjustable bandpass filter with a phase sensitive demodulator (PSD) driven by a chopper drive reference waveform. After filtering, the PSD output is fed into a voltage-to-frequency (v-f) converter that is accurately gated into a 16-bit counter for a 2-s integration period. This approach allows near 16-bit linearity because of the excellent performance of available v-f converters in the frequency range utilized.

The sideband amplifier processes the pressure modulated signal component. It consists of five pole low- and high-pass filters centered on the modulation frequency, a synchronous filter, a PSD driven by a modulator drive reference waveform, a v-f converter, and 16-bit counter. The synchronous filter not only provides additional filtering but also squares the sinusoidal waveform output by the bandpass filter. The PSD output is, therefore, relatively ripple free.

The PMR channels produce wideband and sideband signals, whereas channels 5–9 employ wideband signal processing only. The nine channels have eleven detectors which produce fifteen signals, giving a science data rate of 120 bits/s.

V. Expected Instrument Performance

The expected radiometric performance of each PMIRR channel can be modeled using the mechanical, optical, and electronic design parameters discussed above. This information, when combined with representative retrieval algorithms and Martian atmospheric models, can be used to determine anticipated results for the retrieval of atmospheric parameters at Mars.

A. Radiometric Performance

Table III summarizes the radiometric performance associated with all fifteen PMIRR signals for the spectral channels presented in Table I and the instrument parameters described in Table II. The detector performance figures are based on a study executed by the Santa Barbara Research Center.²² The major parameters are defined as follows:

$$\text{NEdR} = \text{NEP} \times 2^{3/2} / (4/\pi A\Omega WF \sqrt{2T}) \text{ W cm}^{-2} \text{ sr}^{-1} / \text{cm}^{-1},$$

$$\text{SNR} = B(\nu_0, T_0) / \text{NEdR},$$

$$\text{NEdT} = \text{NEdR} / [\text{dB}(\nu_0, T_0) / dT_0] \quad \text{K};$$

$$T_{\min} = B^{-1}(\nu_0, \text{NEdR}) \quad \text{K}.$$

NEdR is the noise equivalent radiance change or the radiative flux that would produce an rms signal referenced to the detector equal to the detector noise equivalent power (NEP). It depends only on detector NEP, instrument etendue ($A\Omega$, $\text{cm}^2 \text{sr}^{-1}$), the equivalent spectral width (W , cm^{-1}), passive optical transmission F associated with each channel, and signal integration time (T , seconds). The SNR depends on NEdR and the target radiance. $B(\nu_0, T_0)$ is the Planck function at the channel central wavenumber ν_0 for a blackbody

Table III. PMIRR Radiometric Performance

CHANNEL(1)	1		2		3		4		5		6		7		8		9(3)	
	PMR	WB	PMR	WB	PMR	WB	PMR	WB	PMR	WB	PMR	WB	PMR	WB	PMR	WB	PMR	WB
CENTRAL WAVELENGTH (cm^{-1})	1315		735		685		1450		845		485		315		215		18,333	
OPTICAL TRANSMISSION	0.46		0.28		0.28		0.38		0.31		0.17		0.14		0.10		0.42	
DETECTOR NEP ($\text{W} \cdot \text{Hz}^{-1/2} \times 10^{13}$)	1.7		4.2		6.7		1.7		3.4		1700		1700		1700		1700	
EQUIVALENT WIDTH (cm^{-1})	0.059	170	0.092	20	5.3	23	0.75	99	50	50	50	50	50	50	50	50	50	50
NOISE EQUIVALENT RADIANCE ($\text{W} \cdot \text{cm}^{-2} \cdot \text{sr}^{-1}/\text{cm}^{-1}$)	9.1 (-9)	1.6 (-12)	2.4 (-8)	5.5 (-11)	6.7 (-10)	7.8 (-11)	8.7 (-10)	3.3 (-12)	1.6 (-11)	1.5 (-8)	1.5 (-8)	1.5 (-8)	1.5 (-8)	1.5 (-8)	1.5 (-8)	1.5 (-8)	1.5 (-8)	1.5 (-8)
SIGNAL TO NOISE RATIO(2)	540 66 1	3.1 (6) 3.8 (5) 5700	600 180 17	2.6 (5) 7.8 (4) 7400	2.2 (4) 7300 810	1.9 (5) 6.2 (4) 6900	4000 390 4	1.1 (6) 1.0 (5) 1000	8.0 (5) 2.0 (5) 1.4 (4)	1000 440 90	600 330 110	270 160 70	3.1 (4) — —	— — —	— — —	— — —	— — —	— — —
NOISE EQUIVALENT TEMPERATURE CHANGE (K)	0.088 0.40 12	1.5 (-5) 7.0 (-5) 2.1 (-3)	0.14 0.26 1.3	3.2 (-4) 6.1 (-4) 2.9 (-3)	3.9 (-3) 6.9 (-3) 0.028	4.6 (-4) 8.2 (-4) 3.3 (-3)	0.011 0.062 2.8	4 (-5) 2.3 (-4) 0.011	9.1 (-5) 2.01 (-4) 1.4 (-3)	0.12 0.16 0.35	0.26 0.30 0.44	0.70 0.75 0.91	— — —	— — —	— — —	— — —	— — —	
MINIMUM DETECTABLE TEMPERATURE (K)	150.1	89.0	107.0	66.3	74.3	64.0	136.9	100.2	69.0	76.3	59.2	50.1	—	—	—	—	—	—

NUMBERS IN PARENTHESES DENOTE EXPONENTS

- (1) PMR AND WB DENOTE PRESSURE MODULATED AND WIDEBAND SIGNALS RESPECTIVELY
- (2) S/N RATIOS AND NOISE EQUIVALENT TEMPERATURE CHANGES ARE CALCULATED FOR THE INSTRUMENT VIEWING BLACKBODIES AT 300, 225 AND 150K
- (3) CHANNEL 9 S/N IS CALCULATED FOR A UNIT ALBEDO LAMBERT SCATTERER AT THE MEAN MARS RADIUS

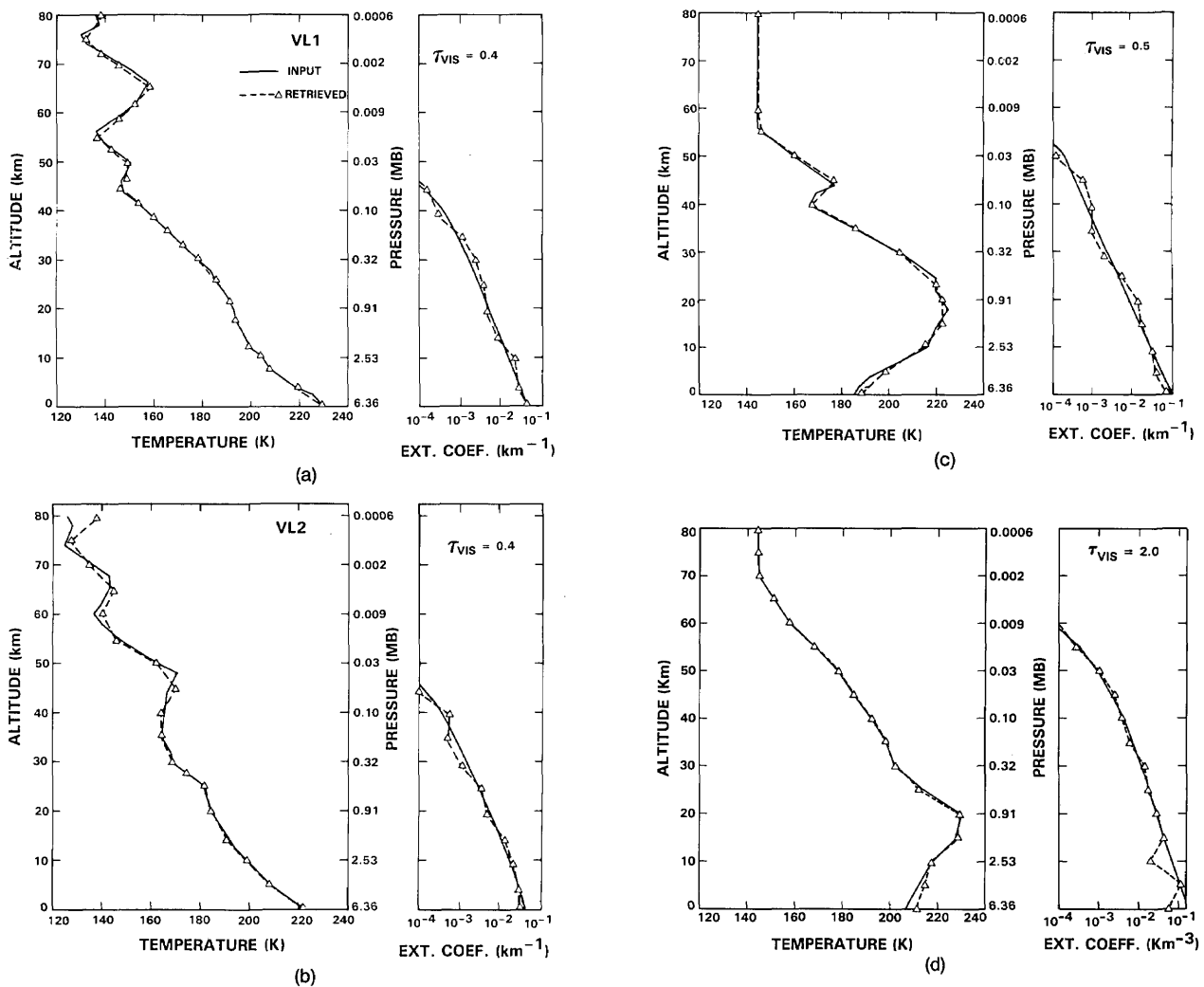


Fig. 11. Comparison of input and retrieved temperature and dust extinction coefficient profiles for input models corresponding to (a) profiles at Viking 1 Lander site; (b) profiles at Viking 2 Lander site; (c) profiles based on the Viking Radio Science experiment; (d) low-latitude, high-dust opacity profiles typical of a global dust storm. All the retrievals use the COSPAR standard atmosphere and uniform dust opacity as a first guess.

target at T_0 K. Similarly, the noise equivalent temperature change (NEdT), or that temperature change which produces a signal change equal to the noise, depends on NEdR and the Planck function derivative. Finally, the minimum detectable temperature T_{\min} , or that temperature which gives a signal equal to the noise, is determined by NEdR and ν_0 . B^{-1} in the above expression indicates the inverse Planck function.

Table III summarizes these parameters for black-body target temperatures that cover the temperature range expected on Mars.

B. Anticipated Results

PMIRR takes an integrated approach to the study of the climate of Mars by simultaneously measuring the vertical profiles of temperature, dust, water vapor, and condensates as a function of pressure in colocated fields of view together with surface brightness tem-

perature and albedo. It acquires these profiles with the one-half scale height vertical resolution needed to determine the 3-D character of the atmospheric fields on daily, monthly, and seasonal time scales. This is done in the presence of the ubiquitous airborne dust and without detailed *a priori* knowledge of aerosol microphysical properties.

The ability of PMIRR to retrieve profiles of atmospheric temperature and constituents simultaneously has been thoroughly tested by numerical simulations. The retrieval schemes used in these simulations employ the iterative relaxation method.^{23,24} A few examples of representative simulations are given below.

The simultaneous retrieval of temperature and dust is illustrated in Figs. 11(a)–(c), which compare input and retrieved temperature and dust profiles. The input profiles are constructed from dust models²⁵ and temperatures measured by the Viking 1 and 2 landers

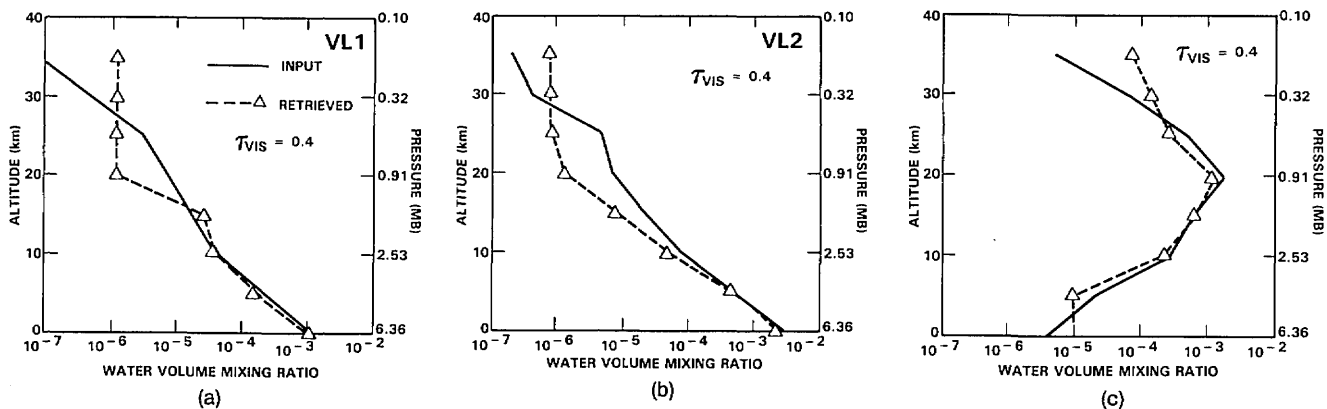


Fig. 12. Comparison of input and retrieved water vapor mixing ratio profiles in the presence of dust for (a) temperature and model mixing ratio profiles at the Viking Lander 1 site; (b) As (a) but at the Viking Lander 2 site; (c) As (a) but based on the Viking radio science experiment.

during entry²⁶ and the Viking orbiter radio science experiment.²⁷ The importance of PMIRR's high vertical resolution is shown clearly in these examples. Below 80 km, temperature errors at 5-km vertical resolution rarely exceed 2 K, and below 50 km dust extinction profiles are retrieved to better than 20%. Dust column abundances are determined with an accuracy of better than 5%.

Figure 12 compares input and retrieved water vapor profiles in dusty atmospheres. The dust models and temperature profiles assumed are those of Fig. 11. Clearly vertical structure in the water vapor profile can be determined below 35 km. Column abundances are generally determined to an accuracy of better than 10% with a lower limit on detection of 10^{-2} pr. μm .

VI. Conclusions

The study of the climate of Mars requires a comprehensive investigation of atmospheric and surface phenomena that are linked by the physical mechanisms of atmospheric transport, surface-atmosphere interaction, radiative heating and cooling, and latent heat exchange. To date, such studies have been severely limited by the lack of simultaneous comprehensive coverage of the distributions of dust, volatiles, and key dynamical fields. From Mars Observer, PMIRR provides global simultaneous spatially coincident vertical profiles of temperature, dust, water vapor, and condensates with additional measurements of surface temperature and polar radiative balance.

PMIRR represents the application to the Martian atmosphere of remote sounding techniques that are now in use broadly in the study of the thermal structure and composition of the terrestrial middle atmosphere on a global scale. In addition to greatly extending our knowledge of the Martian atmosphere, they will yield exciting new comparative data between two atmospheres that share very similar daily and seasonal thermal forcing and will enhance our understanding of the atmospheres of the terrestrial planets.

We would like to acknowledge the contributions made by Burton Zeldin to the thermal aspects of the instrument design.

The research described in this paper was performed by the Jet Propulsion Laboratory, California Institute of Technology, under contract with the National Aeronautics and Space Administration.

References

1. Announcement of Opportunity, Mars Observer Mission, NASA. A.O. OSSA-2-85 (1985).
2. J. C. Gille and J. M. Russell III, "The Limb Infrared Monitor of the Stratosphere: Experiment Description, Performance and Results," *J. Geophys. Res.* **89**, 5125 (1984).
3. J. J. Barnett *et al.*, "Global and Seasonal Variability of the Temperature and Composition of the Middle Atmosphere," *Nature London* **313**, 439 (1985).
4. F. W. Taylor, "Pressure Modulator Radiometry," *Spectrom. Tech.* **4**, 137 (1983).
5. J. T. Houghton and S. D. Smith, "Remote Sounding of Atmospheric Temperature from Satellites, I. Introduction," *Proc. R. Soc. London Ser. A* **320**, 23 (1970).
6. A. K. Smith and L. V. Lyjak, "1985 Observational Estimate of Gravity Wave Drag from the Momentum Balance of the Middle Atmosphere," *J. Geophys. Res.* **90**, 2233 (1985).
7. L. D. Kaplan, "Inference of Atmospheric Structure from Remote Radiation Measurement," *J. Opt. Soc. Am.* **49**, 1004 (1959).
8. J. B. Pollack, D. S. Colburn, F. M. Flasar, R. Kahn, C. E. Carlston, and D. Pidek, "Properties and Effects of Dust Particles Suspended in the Martian Atmosphere," *J. Geophys. Res.* **84**, 2929 (1979).
9. O. B. Toon, J. B. Pollack, and C. Sagan, "Physical Properties of the Particles Composing the Martian Dust Storm of 1971-1972," *Icarus* **30**, 663 (1977).
10. T. Z. Martin, A. R. Peterfreund, E. D. Miner, H. H. Kieffer, and G. E. Hunt, "Thermal Infrared Properties of the Martian Atmosphere I. Global Behaviour at 7, 9, 11 and 20 μm ," *J. Geophys. Res.* **84**, 2830 (1979).
11. R. W. Zurek, "Martian Great Dust Storms: An Update," *Icarus* **50**, 288 (1982).
12. L. L. Gordley and J. M. Russell III, "Rapid Inversion of Limb Radiance Data Using an Emissivity Growth Approximation," *Appl. Opt.* **20**, 807 (1981).

13. G. E. Thomas, B. M. Jakosky, R. A. West, and R. W. Sanders, "Satellite Limb-Scanning Thermal Infrared Observations of the El Chichon Stratospheric Aerosol: First Results," *Geophys. Res. Lett.* **10**, 997 (1983).
14. B. M. Jakosky, "The Seasonal Cycle of Water on Mars," *Space Sci. Rev.* **41**, 131 (1985).
15. H. H. Keiffer, T. Z. Martin, A. R. Peterfreund, B. M. Jakosky, E. D. Miner, and F. D. Palluconi, "Thermal and Albedo Mapping of Mars During the Viking Primary Mission," *J. Geophys. Res.* **4249** (1977).
16. D. A. Paige, "The Annual Heat Balance of the Martian Polar Caps from Viking Observations," Ph.D. Thesis, California Institute of Technology, Pasadena (1985).
17. D. A. Paige and A. P. Ingersoll, "Annual Heat Balance of Martian Polar Caps: Viking Observations," *Science* **228**, 1160 (1985).
18. R. B. Leighton and B. C. Murray, "Behaviour of Carbon Dioxide and Other Volatiles on Mars," *Science* **153**, 136 (1966).
19. J. A. Cunningham and R. A. Mollicone, "Cryogenic Systems for Spaceborne Infrared Applications," *Proc. Soc. Photo-Opt. Instrum. Eng.* **253**, 170 (1980).
20. A. Sherman, "History, Status and Future Applications of Spaceborne Cryogenic Systems," at Cryogenic Engineering Conference, San Diego, CA, 12 Aug. 1981.
21. R. F. Jarnot, "Radiometric Measurement of Minor Atmospheric Constituents," D.Ph. Thesis, U Oxford (1976).
22. Detector focal plane study, Final Report, Santa Barbara Research Center WAL525 (1984).
23. M. T. Chahine, "Inverse Problems in Radiative Transfer: Determination of Atmospheric Parameters," *J. Atmos. Sci.* **27**, 960 (1970).
24. J. Susskind, J. Rosenfield, D. Reuter, and M. T. Chahine, "Remote Sensing of Weather and Climate Parameters from HIRS2/MSU on TIROS-N," *J. Geophys. Res.* **89**, 4677 (1984).
25. B. J. Conrath, "Thermal Structure of the Martian Atmosphere During the Dissipation of the Dust Storm of 1971," *Icarus* **24**, 36 (1975).
26. A. Seiff and D. B. Kirk, "Structure of the Atmosphere of Mars in Summer at Mid-Latitudes," *J. Geophys. Res.* **82**, 4364 (1977).
27. G. F. Lindal *et al.*, "Viking Radio-Occultation Measurements of the Atmosphere and Topography of Mars: Data Acquired During 1 Martian Year of Tracking," *J. Geophys. Res.* **84**, 8443 (1979).

PATENTS PATTERN

Franklin S. Harris, Jr.

This year is the 150th anniversary of the American patent system. The first federal patent law was adopted by the U.S. Congress 10 April 1790 under which all patents were examined personally by the Secretary of State, Thomas Jefferson. Few patents were granted because he was too busy, and the law was changed in 1793 so that a patent was granted by complying with the formal requirements of submitting a description, drawings, and a model without any examination. This led to many patents which were not new and to numerous conflicting patents. On 4 July 1836 the present examination system was adopted which requires that the patent be "new and novel."

Developments of interest relating to optics reported in *NASA Tech Briefs*, **10**, No. 3 (May-June 1986) are given below. Further information can be obtained by writing to the Manager, Technology Transfer Division, P.O. Box 8757, BWI Airport, MD 21240 and giving the identifying number, except in two cases where information can be obtained from the Patent Counsel, (for LAR13336) Howard J. Osborn, Mail Code 279, Hampton, VA 23665, and (for GSC12935) John O. Tresansky, Mail Code 204, Greenbelt, MD 20771.

Laser inertial navigation system

This report describes successful helicopter tests of laser inertial navigational equipment. The tests were conducted over a 3-year period, both in a laboratory and in flight. The inertial system was used as a position/velocity/attitude indicator and later served as part of an automatic flight-control system. The inertial-system sensing head includes integrating laser gyroscopes and linear accelerometers. Each laser gyroscope senses the rotation about a single axis in terms of the phase shift between two laser beams launched along opposite paths about the axis. Each linear accelerometer operates similarly, except that the paths and the sensed motion are along the axis.

There are two variations on the sensing-head design: The triad version has three mutually perpendicular sensing axes, while the tetrad version includes an additional skewed sensing axis along the diagonal of the cube represented by the first three axes. The fourth gyroscope-and-accelerometer set provides redundant sensory data for fault detection and for studies of redundancy management.

The sensing head is of the strapdown type, that is, it is simply mounted in the aircraft and not gimballed. Associated with the sensing head are a control-and-display unit, a system to record flight data, and a dual navigational computer.

The computer program includes provisions for detecting malfunctions in the sensors. As an example, one indication of sensor failure would be that the scalar difference (called the parity residual) between the skewed-sensor output and the vector sum of the orthogonal-sensor outputs exceeds the background noise by a prescribed amount. When a fault is detected in any of the four axes, the sensor data for that axis can be excluded from the navigation calculation, allowing the system to continue operating with the three remaining sensors.

In the flight tests of the triad and tetrad systems, acceptable navigational accuracy was obtained after computer-controlled alignment procedures lasting 5 min or less before each flight. (Alignment is performed with the sensing head in place.) Failure detection using the four-axis parity residual was successful at failure levels far below the noise threshold of flight-sensing requirements.

In the digital navigation-and-control system, the laser inertial equipment provides attitude, position, and velocity information that is combined with information from a microwave landing system and with control signals from the pilot. The processed combination of inputs is fed to the aircraft servo-control system. Such a navigation-and-control system performed well in automatic-flight tests in which a helicopter landed from straight and level flight by first entering a two-turn descending helix, then emerging from the helix in line with a runway, and then decelerating to a hover 4.7 m above the landing point.

This work was done by Ronald J. Hruby and G. Xenakis of Ames Research Center, Ralph A. Carestia of the University of Southern Colorado, William S. Bjorkman and S. F. Schmit of Analytical Mechanics Associates, Inc., and L. D. Corliss of the U.S. Army Aeromechanics Laboratory. Refer to ARC-11473.

Laser cutting of thin nickel bellows

A laser cutting technique produces narrow, precise, fast, and repeatable cuts in thin nickel-alloy bellows material. This technique avoids the distortion, dents, and nicks produced in delicate

continued on page 4260